

Deep Learning Techniques based Non-invasive detection of fasting Blood Glucose Level measurement using Electrochemical Saliva

D. Arul Kumar¹. Dr.T. Jayanthi²

Abstract

In Deep learning methods such as automatic encoder, long-term short-term memory (LSTM) and repetitive neural network (RNN), in mixed group of population, fasting blood glucose level (FBGL) was used to detect the BG level. The Indian population is healthy and sick. The appearance of high FBGL from the electrochemical parameters of human saliva, redox potential, pH, concentration of sodium, and calcium ions was evaluated. Samples were taken from 175 randomly particular persons, half of healthy patients and half of those with diabetes. Models were trained with 70% of all data and tested in the remaining set. In every algorithm, the data points were randomly crossed three times before the model was implemented. The effectiveness of machine learning techniques is presented in terms of the four parameters that are statistically significant, the accuracy, the sensitivity, and the F1 score. The proposed analysis shows that the RNN-based deep learning method yields better results. This deep learning technique to measure blood glucose level non-invasively using electrochemical saliva will help the society to control the diabetes effectively.

Keywords Glucose, Diabetes, Non-invasive GS, self-monitoring Transdermal and optical method.

1. Introduction

After a heart attack and cancer, diabetes presents the third position of most common chronic disease that affects people's health problems [1]. The World Health Organization has announced a global diabetes epidemic that affects 422 million

D. Arul Kumar
arul.annauniv@gmail.com

Dr.T. Jayanthi
jayanthymd@rediffmail.com

¹ Research Scholar, Department of Electronics and Communication Engineering, Sathyabama Institute of Science and Technology, Chennai, India.

² Principal, Panimalar Institute of Technology, Chennai, India.

people worldwide and could pose a serious public health threat in the future. High BG level is basically a chronic illness in which the body cannot produce insulin or use it properly. The human body produces the energy necessary for insulin to absorb glucose contains from the blood. While the insulin sequence is interrupted, glucose does not separate from the blood, which leads to growth [3].

Leaving diabetes untreated can have serious consequences, such as kidney failure, heart defects, and congenital weaknesses [4]. Studies show that online glycemic control lessens complications and extends the lifespan of patients with diabetes by 5–8 years [5]. The most sophisticated glucose measuring using electrochemical test strips need a diabetic to insert his fingers and check blood droplets more number times at a day [6]. This type of test is not only produce pain, but also increases the risk of infection. The reasons given above explain why BG levels are not monitored as recommended many times over the years [7]. Despite important technical problems, he encouraged technologists to introduce non-invasive devices for observing glucose, aimed at alleviating pain and improving access to diabetes [8]. For this purpose, creating a non-invasive method to measuring glucose levels has long been considered the Holy Grail. Optical methods, comprising microwave spectroscopy [9], optical coherence tomography method [10], infrared (NIR) spectroscopy method [11], polarimetry method [12], Raman spectroscopy method [13] and fluorescence technique [14].

Yamakoshi et al. using a spectrograph, 100 sets of NRR spectrum data from 900 to 1700 nm were collected, and SVM was rated as the most accurate according to the reverse analysis of the principal component analysis (PCA), PLS and SVM [15]. An ideal was created that combines multiple linear regression and parallel factor analysis, which is most exact and powerful than multiple linear regressions [16]. Each method has its benefits, but there are also drawbacks: (1) more number of info is captured by independent variable, while these variables can cause the info to be repeated; (2) high precision and fast spectrometers that interfere with the detection of BG in the home; (3) The basic concept of non-invasive technology to detect NIR in NIR is the Bera-Lambert law, which applies to human tissues under appropriate conditions. However, the non-invasive detection of BG NIR does not comply with Bayer-Lambert's law, and the relationship between the NIR signal and the BG measurement is linear and nonlinear. Ficorella et al. pointed out that obtain best presentations in terms of resolution and sensitivity level at 1550 nm [17].

Saliva is a human salivary fluid comprising a mixture of various hormones, enzymes, antibodies, growth factors and antimicrobial components. In fact, most of the compounds that are found in saliva are in the blood, which is very like to serum in regulating the physical condition of the body. It is useful to control salivary markers instead of serum because saliva gathering is a simple and inexpensive procedure that does not cause the patient infection or discomfort. Diabetes mellitus affects saliva, blood flow velocity, infiltration ability, viscosity, electrolytic ion composition and protein level. Therefore, saliva is a sustainable biomarker for categorizing people as diabetics and not. In this article, we measure glucose levels using non-invasive electrochemical saliva for rapid blood determination based on in-depth study methods.

2. Proposed system

In this research, we conducted a brief study of electrochemical changes in saliva gathered from good healthy people and patients with diabetes. The parameters of pH, redox potential (ORP),

individual concentrations, calcium and potassium were compared with the corresponding FBGL standards resolute under similar conditions. In adding to electrochemical factors, age is one of the main variables that evaluate type-2 diabetes mellitus and cardiovascular disease indicators. The 3 numerical scheme based on automatic encoder, long-term memory and RNN were applied to the experiment, which yielded an excellent correlation using saliva as a simple bio fluid to predict FBGL. The proposed model is shown in the Figure 1.

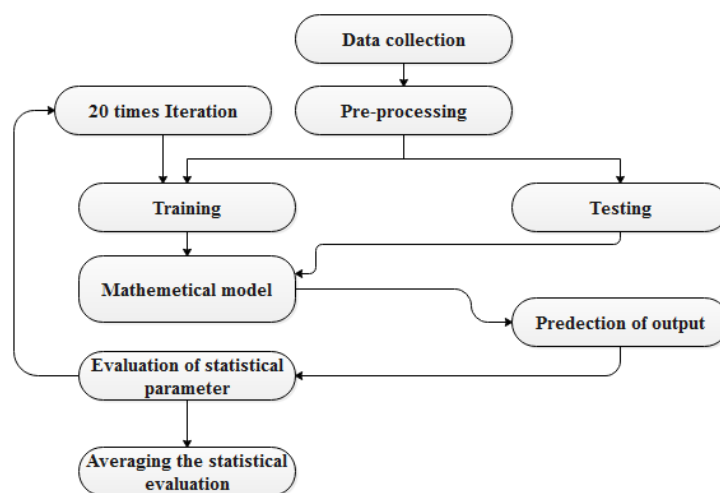


Fig. 1 Proposed model for FBGL detection using electrochemical saliva.

3. Proposed system

3.1 Selection and organization of study groups

An entire of 175 persons aged 18 to 69 years were employed for this paper. Candidates were split into 2 sets: (1) fit being (FBGL): 80–120 mg / dl; 41 women; 46 men; age range 18–62 years; average age 35 ± 11 years , (2) Clinical diagnosis of patients with type-2 diabetes mellitus (FBGL ≥ 120 mg / dl; 47 women; 41 men; age level 21-69 years; average age 47 ± 10 years). After these were omitted from the revision: (1) pathological conditions of saliva, such as salivary stones, mumps, (2) pregnancy, (3) bleeding gums, gingivitis or cancer of the oral cavity, (4) severe diabetic or diabetic complications. (5) Any other systemically ill person, (6) Anti-Topics about drugs, such as cholinergic, sympatometric, skeletal muscle relaxants, anti-migraines, cytotoxic, retinoids and anti-HIV cytokines. An inclusion standard for a pupil with diabetes is based on the references of an expert commission on the diabetes analysis and grouping [18]. These include polydipsia, polyphagia, polyuria, and increased BGL.

3.2 Collection of samples and protocol analysis

Contestants were asked to enter the fast mode from 8:00 am to 10:00 am. Exclude brushing your teeth. They were requested to sit in an isolated room to swallow. They maintained all conditions

and maintained their circadian rhythm. Each person was requested to spit about 2 ml range of saliva into a previously autoclaved collection vessel. These trials of saliva were examined for many electrochemical factors. The pH and redox potential were measured using a pH / ORP meter F-71 Lacqua Lab (Japan). The conductivity and density of the electrolytes (mainly Na +, K + and Ca ++) were recorded using ion selective models of the double series of Horiba Laca. The FBGL vein of all volunteers was calculated in plasma and analyzed using (Cobas Integra 400 Plus) an automatic chemical analyzer compared to the current gold standard.

3.3 Data pre-processing

The electrochemical data got from saliva examples was to train ML algorithms such as automatic encoders, LSTMs, and RNNs to predict the outcome of unknown samples in the future. ML reveals the production methods and trends in big data sets, and is now routinely used in the industry to achieve its goals. Mathematical models were coded in Matlab R2018a. Prior to selecting the data, to attain the normalized data range of -11 to 1, the function of scaling the basic features for all different factors such as pH, ORP, conductivity, electrolyte focus and volunteering in units of measurement parameter. The ratio used to normalize the characteristics is shown in equation 1.

$$x_i' = \frac{x_i - \mu}{\sigma} \quad (1) \quad \text{Here } x_i \text{ denotes what is called the input variable of}$$

the sign (pH, ORP, age, etc.), x_i' is called the normalized variable of the sign, ' μ ' is the average value and ' σ ' is the SD from the complete data obtained. Values of FBGL calculated in venous plasma are classified as 1 (high FBGL) -120 mg/dl, and compared with normalized training set data to control the coefficients of fitting variables associated with the normal equation 2.

$$Y = f_{\theta}(x) \quad (2) \quad \text{Here, predicted output 'Y' FBGL value F of 0 or 1,}$$

x indicates the linear or nonlinear grouping of the input variables, and x is the value of coefficient equal to x .

After normalizing all the data of 175 volunteers, they were randomly generated and cross-validated by splitting them into three sets of randomly generated data. In first two sets were used for the training and another one for the tests.

3.4 Auto Encoder DNN Classifier

The parts in question are classified using the Auto Encoder DNN Classifier based on the selected features. In this research, the automated encoder can be a suitable solution for the proper selection classification process of the DNN when there is no prior knowledge of the distribution data. Auto Encoder DNN usually operates as FFN and is an unsupervised pre-training method with greedy layer-wise training. In DNN, data flow is obtained from the input to the output layer excluding of any looping function. The main benefit of the Auto Encoder DNN Classifier is that the likelihood of low lost value.

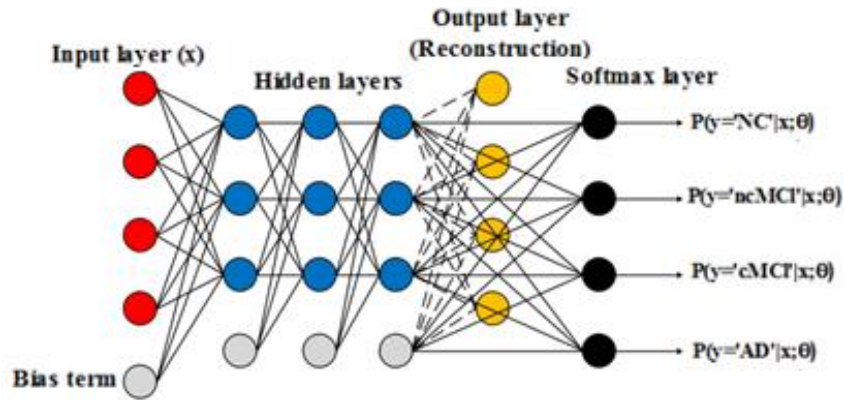


Fig 2 Structure of deep leaning

An automatic encoder is a coding structure composed of a multilayer neural network as shown in figure 2. Input-encoding neurons represent the true input value. Each hidden layer can be seen as a high-level representation of its former fold; however, the true significance of each layer is very small. The cover of the insertion layer is the smallest representation of the insertion layer of the same size as the insertion layer. Activation signals are transferred across the network using equation (3). Until the accrual reaches the exit rate, neuronal activity can be measured using equation (4).

$$\begin{aligned}
 a_{(i)}^{(l)} &= x(i), l = 1 & (3) \quad h(w, b, x) &= a^{(N)} & (4) \\
 a_{(i)}^{(l)} &= \sigma(W^l a + b), l = 1
 \end{aligned}$$

Where ‘x’ represents unlabelled data $\{x^{(i)}\}_{i=1}^m, w = 1$ represents weight matrix controls the activation effect between neurons on the neighbour layer, ‘b’ represents bias term, ‘σ’ represents activation function, it can be set to hyperbolic target function to deliver non-linearity for network to model difficult relationship, and $h(W, b, x)$ represents input data as well as activation output layer. To train this unsupervised ideal, the loss of production is used as an objective function for optimization as given in equation (5).

$$L(W, b, x, z) = \min_{w, b} E(W, b, x, z) + \gamma \|W\|_2^2 + \beta K(W, b, x) \quad (5)$$

Where, $E(W, b, x, z) + \gamma \|W\|_2^2$ signifies the

demonstration loss with squared error. The second term reduces the weight leading to the lower weight, while the third term regulates the sparsity penalty regime ‘β’ with an activation of the target ‘ρ’ near target 0, which imposes a poor representation of the objective function using the Kullback Leibler deviation in all training trials. This is defined in Equation (6).

$$K(W, b, x) = \sum_j^n ID_{KL}(\rho \| \sum_{i=1}^m h_i(x^{(i)}; W, b)) \quad (6)$$

This research simultaneously trains the

hidden layer of the encoder and creates a complete NN by eliminating the temporal output layer. A softmax output layer has been added to the top of the trained self-coding stack, which contains only the previously hidden layer. The softmax layer uses another activation function, which can

be linear, different from the one applied to the previous layer. The softmax activation function is Equation (7).

$$h_i^l = \frac{e^{w_i^l h^{i-1} + b_i^l}}{\sum_j w_j^l h^{i-1} + b_j^l} \quad (7) \quad \text{Where } w_i^l \text{ is the } i\text{th row of } W^l \text{ and } b_i^l \text{ is } i^{\text{th}} \text{ ending}$$

layer bias term. This research can employ h_i^l as an estimator of $P(Y = i|x)$. Where 'Y' is the connected label of input data vector 'x'. In this case, the 4 output neurons in the softmax layer can be interpreted as an AD determinant.

3.5 Long Short Term Memory

In 1997, Hochreiter and Schmidhuber coined the term short-term long-term memory (LSTM). However, there are different versions of LST that researchers currently propose. We provide the details of the LSTM proposed by Zaremba [19]. Assume that 'yt', 'ct' and 'ht' symbolize the input, cell and hidden states respectively, at iteration t. For current input y_t the previous cell state C_{t-1} and its equivalent previous hidden state h_{t-1} , the cell state C_t and hidden state h_t are written as,

$$f, i, o = \sigma(Hy_t + Uh_{t-1} + b) \quad (8)$$

$$j = \tanh((Hy_t + Uh_{t-1}) + b) \quad (9) \quad c_t = f * c_{t-1} + i * j \quad (10)$$

$$h_t = o * \tanh(c_t) \quad (11) \quad \text{Where } * \text{ signifies an element wise multiplication and then vector of bias 'b', and '}\sigma\text{' is a sigmoid function as an activation function,}$$

$$\sigma(x) = 1/(1 + \exp(-x)) \quad (12) \quad \text{The two convolution linear transformation are the H and U then it is applied to } y_t \text{ and } h_{t-1} \text{ respectively and lastly, iteration 't' is } h_t \text{ of the output of an LSTM layer.}$$

3.6 Recurrent Neural Network

RNN is a well-developed ML technology that is renowned for quality in many areas, such as signal processing, NLP, and voice recognition. Unlike traditional neural networks, RNNs explicitly control the temporal dependencies of the data, because the neuron output in T-1 is used to include the next input to power the neuron during t. the neural RNA diagram is shown in Figure 4. From another RNN In the models we have two well-known RNN units - LSTM and Gated Recovery Unit (GRU). Given the size equal to the hidden condition, the LSTM model has extra parameters than the GRU unit defines the architecture of the RNN [20].

4 Results and Discussion

The proposed system was tested with Matlab (version 2018a) with an Intel i5 3.0 GHz processor, drive capacity as 1 TB and size of the RAM as 8 GB. The calculated perfect is used to assess the influence of various parameters on the scheme and predict its performance. Normalizing functions or scaling data is the first phase necessary to undo the effect of certain units. Lastly,

cross-validation helps prevent over-filtering when evaluating classifier performance. Below we discuss the results obtained by filtering the three mathematical models defined in the data of our preparatory test.

4.1. Evaluation Metrics

The result of the system was determined using a confusion matrix (also known as an array of errors or contingencies in deep learning) and receiver performance (ROC). The true positive results (TP) were determined as cases in which the actual and predicted FBGL values were in the range of ≥ 120 mg / dl. Equally, 'tn' value were cases in which both the value of predicted and actual had FBGL < 120 mg / dl. The false positive results (FP) represented cases in which the real state of the infection was false, but the ideal predicted its truth and vice versa for false negative results (FN). The challenge assessment values are used to evaluate the separation and classification performance. For partitioning, the evaluation criteria included accuracy (AC), recall (R) and accuracy (P). The performance standards are as trails:

$$AC = \frac{tp + tn}{tp + fp + tn + fn} \quad (13)$$

$$P = \frac{tp + tn}{tp + tn + fp + fn} \quad (14)$$

$$R = \frac{tp}{tp + fn} \quad (15)$$

4.2. Results

This section delivers the performance result of our model. In the Table 2, it shows outcomes of various classification approaches. Also, displaying the average and SD values of accuracy (AC) Recall (R) and Precision (P) metrics from 3 repetitions. In the table.1, the proposed system performances are validated with some of the ML techniques such as, LLR, ANN, Linear-SVM and RBF-SVM for all classifier performance index (CPI) parameters obtained after 20 repetitions.

Table 1 The average and SD from cross-validation 5 times on the data with ML technique

Classifier	AC	R	P
LLR	75.86	75.48	76.76
ANN	80.7	79.3	81.2
Linear-SVM	77.93	79.43	77.59
RBF-SVM	84.09	84.92	83.75

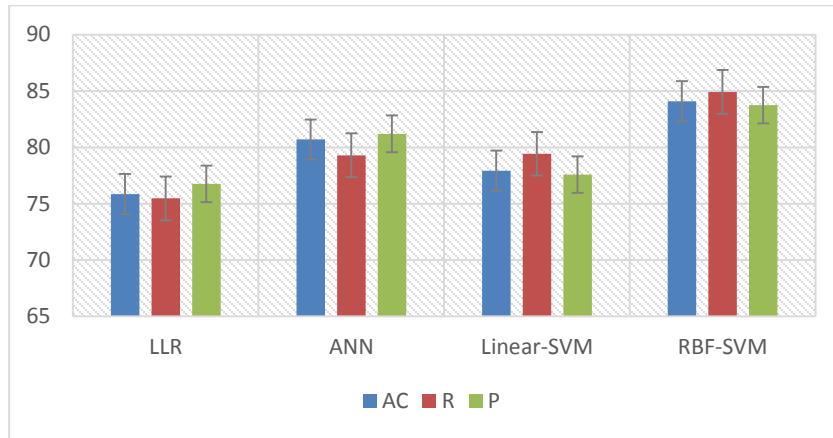


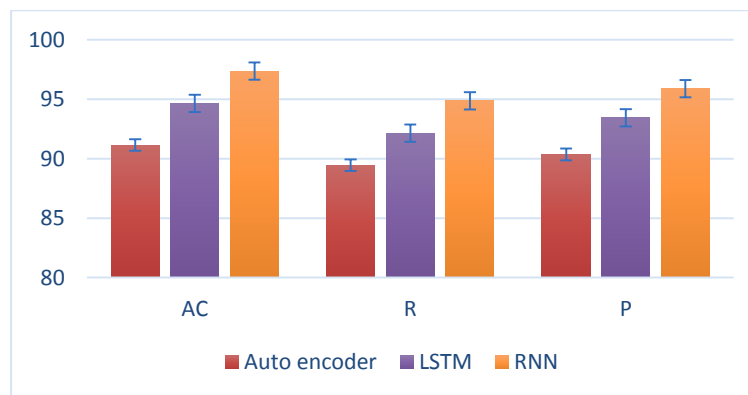
Figure 3 Comparative analysis for various ML techniques

In above table. 1 and figure. 3 shows the comparative analysis of various ML techniques. Here we used various classifiers to analysis the accuracy, recall and precision. Initially LLR and ANN techniques used to analysis the parameter. The ANN outcome performance is better than the LLR. Then the linear-SVM also attained better result such as accuracy is 77.93 and recall is 77.93 and precision is 77.59. After we proposed the method of RBF-SVM is used. It achieved the higher outcome performance such as accuracy level is 84.09, recall is 84.92 and the precision is 83.75. Our novel method is better than the previous methods results.

Table 2. The average and SD from cross-validation 5 times on the data with various Deep learning techniques.

Classifier	AC	R	P
Auto encoder	91.15	89.45	90.35
LSTM	94.64	92.14	93.44
RNN	97.35	94.85	95.87

Figure 3 Comparative analysis for various Deep learning techniques.



In above table 2 and figure 3 displays an average and SD from cross-validation with various Deep learning practices, also comparative analysis of various deep learning techniques. The auto encoder classifier to get the output performance of accuracy as 91.15, recall as 89.45 and

- [8].Omid, V.; Tang, B.C.; Whitehead, K.A.; Anderson, D.G.; Robert, L. Managing diabetes with nanomedicine: challenges and opportunities. *Nat. Rev. Drug Discov.* 2015, 14, 45
- [9].Foroughi F, Rahsepar M, Hadianfard MJ, Kim H. Microwave-assisted synthesis of graphene modified CuO nanoparticles for voltammetric enzyme-free sensing of glucose at biological pH values. *Microchimica Acta.* 2018 Jan 1; 185(1):57.
- [10].Lan, Y.T.; Kuang, Y.P.; Zhou, L.P.; Wu, G.Y.; Gu, P.C.; Wei, H.J.; Chen, K. Noninvasive monitoring of blood glucose concentration in diabetic patients with optical coherence tomography. *Laser Phys. Lett.* 2017, 14, 035603.
- [11].Maruo, Katsuhiko, et al. "New methodology to obtain a calibration model for noninvasive near-infrared blood glucose monitoring." *Applied spectroscopy* 60.4 (2006): 441-449.
- [12].Yu, Z.F.; Pirstill, C.W.; Coté, G.L. Dual-modulation, dual-wavelength, optical polarimetry system for glucose monitoring. *J. Biomed. Opt.* 2016, 21, 087001.
- [13].Lundsgaardnielsen, S.M.; Pors, A.; Banke, S.O.; Henriksen, J.E.; Hepp, D.K.; Weber, A. Critical-depth Raman spectroscopy enables home-use non-invasive glucose monitoring. *PLoS ONE* 2018, 13, e0197134.
- [14].Sylvie, B.; Jean Marie, D.; Serge, M. Noninvasive fluorescent study in situ and in real time of glucose effects on the pharmacokinetic of calcein. *J. Biomed. Opt.* 2002, 7, 609.
- [15].Yamakoshi Y, Ogawa M, Tamura T. Multivariate regression and classification models for estimation of blood glucose levels using a new non-invasive optical measurement technique named pulse-glucometry. *Open Optics Journal* 2009; 3(1): 63-69(7).
- [16].Zhang W, Liu R, Xu K. Enhanced robustness of calibration models using parallel factor (PARAFAC) analysis with NIR spectral data for non-invasive blood glucose monitoring. *ACTA Chimica Sinica* 2013; 71(9): 1281-1286.
- [17].Dai J, Ji Z, Du Y, Chen S. In vivo noninvasive blood glucose detection using near-infrared spectrum based on the PSO-2ANN model. *Technology and Health Care.* 2018 Jan 1;26(S1):229-39.
- [18].Yang X, Ji Z, Yang L, Peng C. The construction and analysis of the optical system for non-invasive blood glucose detection based on near infrared transmission method. *Chinese Journal of Biomedical Engineering* 2012; 1: 147-150.
- [19].Omer, A.E., Safavi-Naeini, S., Hughson, R. and Shaker, G., 2020. Blood Glucose Level Monitoring Using an FMCW Millimeter-Wave Radar Sensor. *Remote Sensing*, 12(3), p.385.
- [20].W. Zaremba and Ilya S., O. Vinyals Recurrent Neural Network Regularization *Xiv:1409.2329v5*, 2015.